Chinese Chemical Letters 36 (2025) 109834

Contents lists available at ScienceDirect

Chinese Chemical Letters

journal homepage: www.elsevier.com/locate/cclet

NIR-II fluorescence lateral flow immunosensor based on efficient energy transfer probe for point-of-care testing of tumor biomarkers

Zhaorui Song[a,1], Qiulian Hao[a,1], Bing Li[c], Yuwei Yuan[d], Shanshan Zhang[a], Yongkuan Suo[a,b,e,*], Hai-Hao Han[a,b,d,e,*], Zhen Cheng[a,b,c,e,*]

[a] Shandong Laboratory of Yantai Drug Discovery, Bohai Rim Advanced Research Institute for Drug Discovery, Yantai 264117, China
[b] State Key Laboratory of Drug Research, Molecular Imaging Center, Shanghai Institute of Materia Medica, Shanghai 201203, China
[c] Institute of Molecular Medicine Joint Laboratory for Molecular Medicine Northeastern University, Shenyang 110000, China
[d] Pharmacy College, Shandong First Medical University & Shandong Academy of Medical Sciences, Ji'nan 250117, China
[e] University of Chinese Academy of Sciences, Beijing 100049, China

ARTICLE INFO

Article history:
Received 23 November 2023
Revised 26 February 2024
Accepted 25 March 2024
Available online 26 March 2024

Keywords:
Donor-acceptor energy transfer (ET)
Lateral flow immunoassay (LFA)
The second near-infrared (NIR-II) fluorescence
Rare-earth nanoparticles (RENPs)
Poly(lactic acid-*co*-glycolic acid) (PLGA)
Tumor biomarker

ABSTRACT

Fluorescence lateral flow immunoassay (LFA) has emerged as a powerful tool for rapid screening of various biomarkers owing to its simplicity, sensitivity and flexibility. It is noteworthy that fluorescent probe mainly determines the analytical performance of LFA. Due to the emission and excitation wavelengths are located in the visible region, most fluorophores are inevitably subject to light scattering and background autofluorescence. Herein, we reported a novel LFA sensor based on the second near-infrared (NIR-II) fluorescent probe with excellent anti-interference capability. The designed NIR-II probe was the Nd^{3+} and Yb^{3+} doped rare earth nanoparticles (RENPs) by employing Nd^{3+} as energy donor and Yb^{3+} as energy acceptor, which of the donor-acceptor energy transfer (ET) efficiency reached up to 80.7%. Meanwhile, relying on the convenient and effective encapsulation strategy of poly(lactic-*co*-glycolic acid) (PLGA) microspheres to RENPs, the surface functionalized NIR-II probe (RE@PLGA) was obtained for subsequent bioconjugation. Benefiting from the optical advantages of NIR-II probe, this proposed NIR-II LFA displayed a good linear relationship ranging from 7 ng/mL to 200 ng/mL for the detection of α-fetoprotein (AFP), an important biomarker of hepatocellular carcinoma (HCC). The limit of detection (LOD) was determined as low as 3.0 ng/mL, which was of 8.3 times lower than clinical cutoff value. It is promising that LFA sensor based on this efficient RENPs probe provides new opportunities for high sensitive detection of various biomarkers in biological samples.

Fluorescent lateral flow immunoassay (LFA) as the most common point-of-care testing (POCT) platform has attracted considerable attentions due to their advantages of rapidity, simplicity and low-cost [1–3]. It is worth emphasizing that fluorescence reporter mainly determines the analytical performance of LFA. Despite great efforts that have been devoted to develop numerous fluorescent probes, such as fluorescent organic dyes, quantum dots (QDs), upconversion nanoparticles (UCNPs), fluorescent probes reported so far generally have relatively poor performance caused by emission light located in the visible region (400–700 nm) [4–6]. These fluorescent probes usually suffer from relative low sensitivity and signal-to-noise ratio (S/N) owing to their higher light absorption as well as undesired autofluorescence from endogenous fluorophores (whole blood, plasma, urine, *et al.*) and nitrocellulose (NC) membrane of LFA, which are unfavorable for monitoring low-concentrated targets [7–9].

Fluorescence detection in the second near-infrared window (NIR-II, 1000–1700 nm) has special superiority because of the low scattering and background autofluorescence [10–13]. Among the numerous NIR-II fluorescent probes, rare-earth nanoparticles (RENPs) feature unique characteristics, such as large Stokes shift (>200 nm), large absorption cross-section, sharp emission band, superior photostability, good chemical durability and ease of surface modification [14,15]. Although we have recently reported a new-type NIR-II LFA platform based on RENPs probe ($NaYF_4$:7%Nd@$NaYF_4$) for the detection of tumor biomarker in biological samples [16], RENPs probes used at present still encounter two inevitable problems in practical applications. (1) In this only

* Corresponding authors at: Shandong Laboratory of Yantai Drug Discovery, Bohai Rim Advanced Research Institute for Drug Discovery, Yantai 264117, China.
E-mail addresses: suoyongkuan@simm.ac.cn (Y. Suo), hanhaihao@simm.ac.cn (H.-H. Han), zcheng@simm.ac.cn (Z. Cheng).
[1] These authors contributed equally to this work.

https://doi.org/10.1016/j.cclet.2024.109834
1001-8417/

Nd^{3+}-doped RENPs, Nd^{3+} was employed as both the sensitizer and activator. NIR-II fluorescence emission based on the only Nd^{3+}-doped RENPs was realized through the intrinsic emission from Nd^{3+} after absorbing the excitation photons [14,17]. Due to Nd^{3+} had multiple excited states, the only Nd^{3+}-doped RENPs showed unsatisfactory fluorescence quantum yield (QY <10%) [18]. (2) the surface hydrophilic modification of RENPs is an absolutely essential part in the construction of LFA. However, it also remains a bottleneck to develop practical strategy to achieve surface hydrophilicity conversion. The common surface modification strategy was ligand exchange, suffering from the weaknesses of tedious and time-consuming treatment process, unavoidable aggregation of bare RENPs, leading to the decrease of luminescence intensity in some degree [19–23]. To further solve these problems for improving the performance of NIR-II LFA, it still needs to take lots of efforts to develop diverse strategies for designing more efficient NIR-II fluorescent probes.

In this work, we designed and synthesized an efficient NIR-II probe based on the Nd^{3+} and Yb^{3+} doped RENPs by employing Nd^{3+} as energy donor and Yb^{3+} as energy acceptor. Due to the high energy transfer process from sensitizer ion Nd^{3+} to emitter ion Yb^{3+}, this RENPs probe exhibited high ET efficiency and anti-interference capacity of background fluorescence. Meanwhile, relying on the convenient and efficient encapsulation action of PLGA microspheres to RENPs, the surface functionalized NIR-II probe (RE@PLGA) was obtained for subsequent bioconjugation. By employing RE@PLGA as the fluorescent reporter, a novel NIR-II LFA sensor was developed to detect α-fetoprotein (AFP), one kind of extremely important biomarkers for the diagnosis of hepatocellular carcinoma (HCC) [24]. The proposed NIR-II LFA possessed advantages of high sensitivity, good reliability and rapid response. It is expected to be a powerful technique for POCT, which will further manifest its values in primary care, rapid diagnosis and massive screening.

Previous researches have shown that it has high efficiency of energy transfer (up to 70%) between sensitizer ion Nd^{3+} and emitter ion Yb^{3+} in the Nd^{3+}-sensitized Yb^{3+} system [25–27]. According to previous report, we synthesized the Nd^{3+} and Yb^{3+} doped RENPs with some modifications [22]. The schematic structure of RENPs presented an obvious core-shell structure, and its structural components were $NaYbF_4$@$NaYF_4$:Nd70%@$NaYF_4$ (denoted as Yb@Y-Nd70%@Y) (Fig. 1a). Especially, $NaYbF_4$ NPs, which acted as the only activators, were located in the inner core and could quickly receive energy from Nd^{3+} ions. Due to Nd^{3+} ion had a higher absorbance coefficient than Yb^{3+} ion, it served as the efficient light absorber and sensitizers, and its doping concentration was regulated over a large range (from 30% to 95%) [22]. To avoid harsh cross-relaxation effect by excessive doping concentration, the optimal doping concentration of Nd^{3+} ions (Nd70%) were distributed in the secondary outer layer ($NaYF_4$:Nd70%). Furthermore, $NaYF_4$ was coated at the outermost layer to protect inner sensitizer and activator from surface quenching.

The inner ET process of RENPs (Yb@Y-Nd70%@Y) probe was confirmed by the changes of NIR absorption spectra and fluorescence emission spectra of lanthanide ions (Nd^{3+}/Yb^{3+})-doped RENPs. Absorption spectra of RENPs (Yb@Y-Nd70%@Y) showed three NIR absorption peaks, which located at 730, 796 and 865 nm, corresponding to transition from $4I_{9/2}$ state to $4F_{7/2}$, $4F_{5/2}$, and $4F_{3/2}$ states (Fig. 1b), and its NIR-II fluorescent emission peak appeared at ~980 nm with 1.34-fold higher luminous intensity than that of RENPs (Yb@Y-Nd70%) under excitation of 808 nm laser (Fig. 1c). NIR emission peaks of the only Nd^{3+}-doped RENPs (Y-Nd70%) were separately at 865 nm ($4F_{3/2}\rightarrow4I_{9/2}$), 895 nm ($4F_{3/2}\rightarrow4I_{11/2}$), 1064 nm ($4F_{3/2}\rightarrow4I_{13/2}$) and 1332 nm ($4F_{3/2}\rightarrow4I_{15/2}$) under the excitation of 808 nm light (Fig. 1d) [28,29]. $NaYbF_4$ showed no fluorescence emission peak in NIR-II region under 808 nm excitation. However, a complete disappearance in fluorescence emission peak (1064 nm) from Nd^{3+} ions and simultaneous appearance of fluorescence emission peak at ~980 nm from Yb^{3+} ions were observed in RENPs (Yb@Y-Nd70%@Y), and its NIR emitting brightness was 2.85-fold higher than that of the only Nd^{3+}-doped RENPs (Y-Nd70%) at the same testing conditions (Fig. 1d). This phenomenon illustrated that the absorbed energy from the excitation light by Nd^{3+} ions have been effectively transferred to Yb^{3+} ions.

Occurrence mechanism of ET between Nd^{3+} ion and Yb^{3+} ion was further explored. Absorption spectra of $NaYbF_4$ revealed an obvious NIR absorption peak at ~980 nm and the relative large absorption cross-section from 900 nm to 950 nm, respectively. Because there was an obvious spectral overlap between Nd^{3+} emission region and Yb^{3+} absorption region, it strongly favored Nd^{3+}-to-Yb^{3+} energy transfer (Fig. 1e). The ET efficiency (E_{ET}) was defined as the percent of energy transferring from the donor (Nd^{3+} ion) to acceptor (Yb^{3+} ion) [30], and it was calculated as 80.7% for RENPs (Yb@Y-Nd70%@Y) (Fig. 1f), which was far higher than that of the most commonly used ET system [31]. More specifically, the photoluminescence (PL) process of RENPs (Yb@Y-Nd70%@Y) probe based on the inner ET mechanism was further described as follows: Thanks to large absorption cross-section of Nd^{3+} ions, high Nd^{3+}-doped nanocrystals (Nd70%) as an efficient energy donor could absorb the excitation energy under 808 nm laser excitation, and then Nd^{3+} transferred photons with the generation of electrons from the $4I_{9/2}$ ground state to the $4F_{5/2}$, followed by a non-radiation transition to its $4F_{3/2}$ state. The emission energy was effectively transferred to the energy acceptor Yb^{3+} *via* $4F_{3/2}$ (Nd^{3+}) + $2F_{7/2}$ (Yb^{3+}) → $4I_{9/2}$ (Nd^{3+}) + $2F_{5/2}$ (Yb^{3+}), and then populated the $2F_{5/2}$ state of Yb^{3+}, generating strong FL emission at ~980 nm (Fig. 1g) [17,22].

The synthesized RENPs were surface-modified by the convenient and effective encapsulation strategy of PLGA microspheres for bioconjugation. The preparation process of RE@PLGA microspheres was displayed in Supporting information (Figs. S1 and S2 in Supporting information), and it was further characterized by different techniques. TEM images showed the typical features of RENPs, PLGA and RE@PLGA microspheres. RENPs core ($NaYbF_4$) exhibited a regular spherical structure (Figs. 2a and b) and the average particle size was determined as 6.8 nm by the dynamic light scattering (DLS) (Fig. S3a in Supporting information). The average diameter of RENPs (Yb@Y-Nd70%) was detected as 13.5 nm by DLS, and it could be calculated that the inner shell thickness (Y-Nd70%) was about 6.7 nm (Fig. S3b in Supporting information), which well meets the spatial distance requirement (<10 nm) of ET. TEM image of RENPs (Yb@Y-Nd70%@Y) also displayed a monodisperse spherical structure (Figs. 2c and d) with the average particle size 25.0 nm measured by DLS, which could be confirmed that the outer coating thickness ($NaYF_4$) was about 11.5 nm (Fig. S3c in Supporting information). TEM image of PLGA microsphere showed regular sphericity with an internal cavity (Fig. 2e), and its average diameter was 121.1 nm detected by DLS (Fig. S3d in Supporting information). For RE@PLGA microspheres, it was obviously seen that one or more RENPs (n = 1–4) had been encapsulated at the cavity of PLGA microspheres (Fig. S4 in Supporting information), and the formed RE@PLGA microspheres displayed relatively irregular spherical structure (Fig. 2f) with the mean size of 180 ± 40 nm (Fig. S3e in Supporting information). Moreover, the zeta potential of PLGA and RE@PLGA were -6.8 mV and -4.1 mV ± 1.5 mV, respectively (Fig. S5 in Supporting information). Negative potentials of two kinds of microspheres were due to the presence of carboxyl groups on the surface. After modification with AFP detection antibody, the hydrodynamic di-

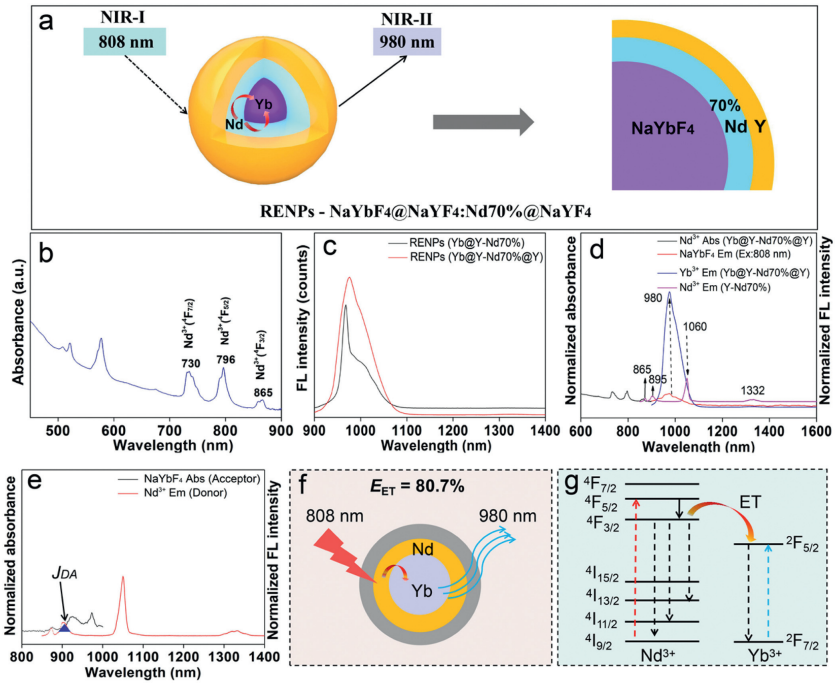

Fig. 1. The inner ET mechanism of RENPs probe (Yb@Y-Nd70%@Y). (a) Structure illustration of RENPs. (b) Absorbance spectrum of RENPs, demonstrating multiple absorbance peaks including one at ~800 nm. (c) Fluorescence emission spectra of RENPs with FL emission peaks at ~980 nm, which were obtained using an 808 nm excitation laser. (d, e) Normalized NIR absorption and emission spectra of the only Nd^{3+}-doped RENPs (Y-Nd70%), the only Yb^{3+}-doped RENPs ($NaYbF_4$) and the Nd^{3+} and Yb^{3+} doped RENPs (Yb@Y-Nd70%@Y), respectively. The shaded region J_{DA} represented the overlap region between the Nd^{3+} emission and the Yb^{3+} absorption spectra. (f) ET efficiency of RENPs. (g) Schematic illustration of ET mechanism between Nd^{3+} ion and Yb^{3+} ion of RENPs in the inner of RENPs probe.

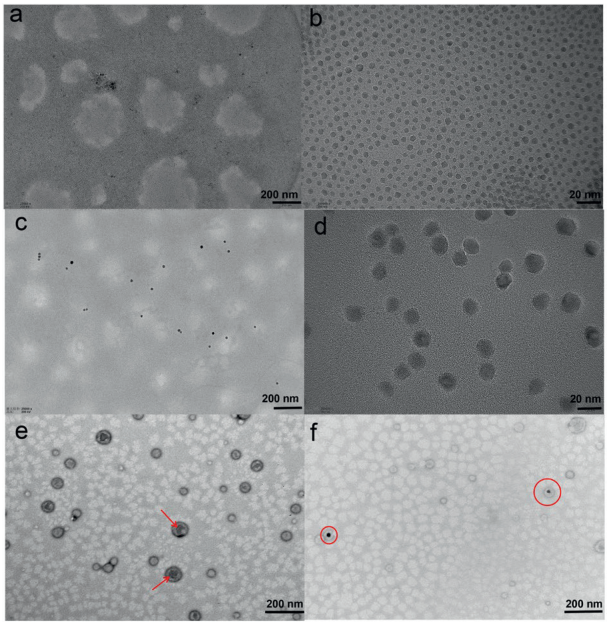

Fig. 2. Morphology characterization of RENPs and RE@PLGA. (a, b) TEM image of $NaYbF_4$. (c, d) TEM image of RENPs (Yb@Y-Nd70%@Y). (e) TEM image of PLGA microspheres. Red arrow points to its inner cavity. (f) TEM image of RE@PLGA microspheres.

ameter of RE@PLGA-Ab reached 588.8 nm and its zeta potential was -9.46 mV, exhibiting obvious changes (Fig. S6 in Supporting information).

The surface structure of RE@PLGA was firstly confirmed by Fourier infrared transform spectroscopy (FT-IR), which was shown in Supporting information (Fig. S7 in Supporting information). Moreover, the chemical compositions of RE@PLGA were further confirmed by energy dispersive X-ray (EDX) spectroscopy. It was clear that RE@PLGA contained C, O, F, Y, Nd and Yb elements. The inset table exhibited the contents of every element. Elemental mapping images revealed that three elements (F, Y and Nd) were brightly colored, demonstrating the existence of these elements at the outer shell of RENPs. Yb element looked dull in color, confirming it lied in the core of RENPs. C and O elements were relatively evenly distributed, indicating that the coexistence of RE@PLGA and PLGA microspheres (Fig. S8 in Supporting information). Furthermore, RE@PLGA microspheres also exhibited excellent physical stability and photostability (Fig. S9 in Supporting information). Encapsulation efficiency (EE) of PLGA microspheres to RENPs reached 88.8%, which provided a convenient and efficient encapsulation strategy (Fig. S10 in Supporting information).

Principle of NIR-II probe-based LFA was explained as follows: With the high ET efficiency and superior optical performance, RENPs (Yb@Y-Nd70%@Y) probe is critical for realizing high-sensitive and accurate detection of tumor biomarkers in that it is able to avoid the background interference from biological samples. From Scheme 1, AFP coating antibodies (AFP-09) set as test line (T line) and IgG as control line (C line) had been sprayed on the nitrocellulose (NC) membrane, respectively. Biological samples containing AFP and RE@PLGA-Ab solution were premixed and then added into the sample well of detection card, followed by adding with sample buffer. Sample liquid flew along the test strip to the NC membrane, and the formed immune complex (RE@PLGA-Ab-AFP-10) specifically reacted with AFP coating antibody, forming a sandwich structure (RE@PLGA-Ab-AFP-AFP09) at T line. The surplus RE@PLGA-Ab complex was non-specifically bound to IgG immobilized on the C line as a quality control signal. Under the excitation light of 808 nm, the generated NIR-II fluorescent emission signals (980 nm) at T line and C line were recorded by NIR-II fluorescence immune analyzer, respectively. Under the optimal conditions, AFP concentrations and ratios (T/C) of FL intensity at 980 nm presented

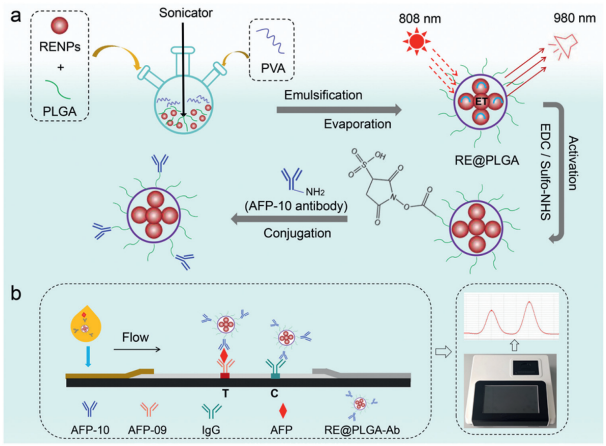

Scheme 1. Design scheme of LFA sensor based on the efficient NIR-II probe. (a) Preparation progress of RE@PLGA microsphere and its antibody conjugation process. (b) Schematic diagram describing NIR-II LFA for detection of AFP.

a good linear relationship, which would provide a rapid, sensitive and accurate method for the quantitative detection of AFP in biological samples.

Optimization of immunoreaction condition is the key parameter to improve the detection performance of NIR-II LFA, and the detailed progress had been displayed in Supporting information (Figs. S11-S17 in Supporting information). Under the optimal conditions, a novel LFA sensor based on the efficient NIR-II probe was developed for the determination of AFP. As the increasing concentrations of AFP, the fluorescence intensity ratio (T/C) increased gradually. AFP concentrations and T/C values displayed a good linear relationship from 7.0 ng/mL to 200 ng/mL ($y = 0.0023x + 0.0413$, $R = 0.9923$) (Figs. 3a–c). The limit of detection (LOD) was estimated to be 3.0 ng/mL, which was of 8.3 times lower than the clinical cut-off values (25 ng/mL) (Fig. 3d) [32]. Moreover, compared with previously reported detection methods, the proposed NIR-II LFA also exhibited good sensitivity and relative wide linear detection range (Table S1 in Supporting information).

The specificity of NIR-II LFA was estimated by adding four kinds of tumor biomarkers (AFP, CEA, PSA and CA50), respectively. The cross reactivity (CR) was calculated to assess the specificity of the method. When high concentration of tumor biomarkers (200 ng/mL) were added into the prepared NIR-II LFA test strips, only the T/C value of AFP was high (0.534). T/C values of other tumor biomarkers (CEA, PSA, CA50) were below 0.02, and the corresponding CR were also no more than 1.5%. It indicated that these interfering substances had little effect on the detection process of NIR-II LFA, exhibiting excellent specificity (Fig. 3e). Owing to the selective recognition ability of antibody mainly determined the specificity of method, it also proved that the prepared NIR-II probe (RE@PLGA-Ab) possessed good selectivity.

The reproducibility of NIR-II LFA was evaluated by recovery rates, intraday and interday variations. From Table S2 (Supporting information), the recovery rates from the mimical serum samples spiked with different concentrations of AFP ranged from 93.6% – 110.6% with coefficients of variation (CV) below 10%, and the interday CV was also lower than 14%, indicating excellent accuracy and precision. In addition, the prepared NIR-II LFA test strips were placed at oven (45 °C, 7 days) to explore the storage stability. From Table S3 (Supporting information), the recovery rates ranged from 90.0% to 108.5% in 7 days at high ambient temperature (45 °C). Meanwhile, the intraday CV was lower than 10.0% and the interday CV was also no more than 15.0%. These results showed that the prepared NIR-II LFA test strips had good stability and durability.

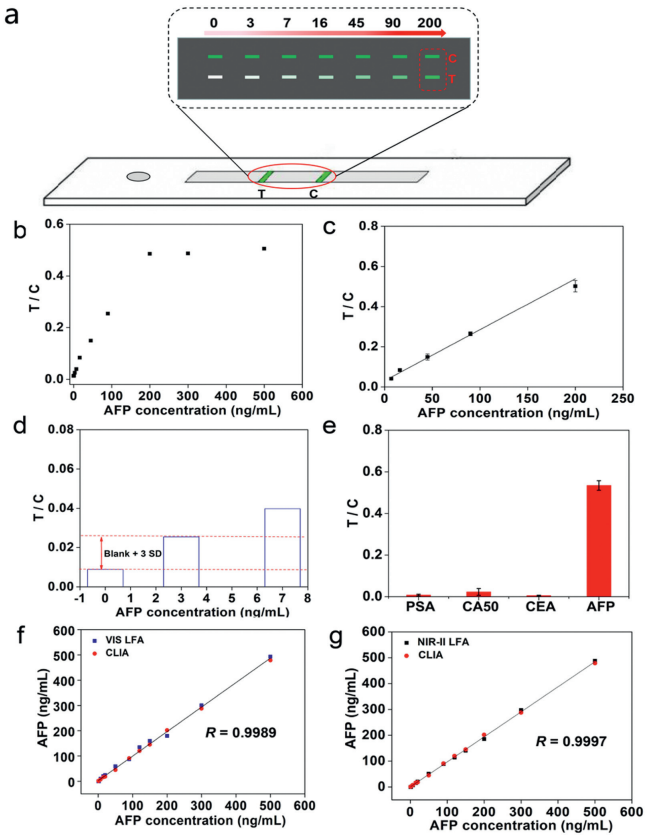

Fig. 3. Analytical performance of LFA sensor based on the efficient NIR-II fluorescent probe. (a) NIR-II imaging of LFA test strips with different concentrations of AFP from 0 to 200 ng/mL. (b) T/C value changes with increasing concentrations of AFP. (c) Calibration curve for T/C values *versus* AFP concentrations ($n = 5$). (d) The limit of detection of NIR-II LFA. It was calculated by the blank intensity plus three folds standard deviation. (e) Analytical specificity of NIR-II LFA towards AFP and other tumor biomarkers ($n = 5$). (f) Correlation coefficient between Roche CLIA and the VIS LFA method. (g) Correlation coefficient between Roche CLIA and the developed NIR-II LFA method.

Chemiluminescent immunoassay (CLIA) was employed as control to further evaluate the validity and reliability of NIR-II LFA. Twelve serum samples determined by Roche CLIA (linear range: 0.5–1000 ng/mL), the commercial AFP kit (linear range: 10–200 ng/mL, detection with visible fluorescence) and the proposed NIR-II LFA method (linear range: 7.0–200 ng/mL), respectively. The sample test results were firstly carried out a statistical analysis by SPSS software. It showed that whether the NIR-II LFA and CLIA or the VIS LFA and CLIA, there were no significant differences ($P > 0.05$), which indicated that the developed NIR-II LFA for AFP detection is reliable. The consistency analysis of test results of three methods was further carried out. From Figs. 3f and g, the correlation coefficient (R) between VIS LFA and CLIA was 0.9989, and the correlation coefficient between NIR-II LFA and CLIA reached 0.9997. Compared with VIS LFA, the developed NIR-II LFA was in better agreement with CLIA, which indicated that the proposed LFA sensor based on the efficient NIR-II probe has more excellent accuracy and validity in the quantitative determination of AFP in clinical serum samples.

In summary, we have developed a novel LFA sensor based on the efficient NIR-II fluorescent probe for detection of tumor biomarkers (AFP as a model analyte). The proposed RENPs probe possesses three unique advantages, giving great prospects for clinical translation. Firstly, the low preparation cost and the controllable preparation progress make it easy for large-scale production. Secondly, the sensitizer ions Nd^{3+} and emitter ions Yb^{3+} con-

structed an energy transfer highway in the inner of RENPs, generating excellent fluorescence efficiency. Thirdly, the encapsulation strategy of PLGA microspheres easily realized the surface modifications of RENPs, which will contribute to bioconjugation. Thanks to its superior anti-interference capability and fluorescence property of NIR-II probe, the proposed NIR-II LFA sensor has the ability to realize background-free detection of tumor biomarkers in clinical serum sample with good sensitivity and wide linear range. This LFA sensor can serve as a powerful tool for early diagnosis and mass screening of tumor biomarkers in POCT.

Declaration of competing interest

The authors declare that they have no known competing financial interests or personal relationships that could have appeared to influence the work reported in this paper.

Acknowledgments

This work was supported by the National Natural Science Foundation of China (Nos. U2267221, 22107029, 22377135), the Bohai Rim Advanced Research Institute for Drug Discovery (No. LX215002), the Natural Science Foundation of Shandong Province (No. ZR2022QH212), the Taishan Scholars Program (No. tsqn202312305), the Young Elite Scientists Sponsorship Program by Chinese Chemical Society, the Fundamental Research Projects of Science & Technology Innovation and development Plan in Yantai City (No. 2023JCYJ059), the Shandong Laboratory Program (No. SYS202205) and the Shanghai Postdoctoral Excellence Program (No. 2023704).

Supplementary materials

Supplementary material associated with this article can be found, in the online version, at doi:10.1016/j.cclet.2024.109834.

References

[1] Z. Qin, T.B. Ren, H. Zhou, et al., Angew. Chem. Int. Ed. 61 (2022) e202201541.
[2] Z. Wang, K. Xing, N. Ding, et al., J. Hazard. Mater. 423 (2022) 127204.
[3] W. Wang, X. Yang, Z. Rong, et al., Nano Res. 16 (2023) 3063–3073.
[4] L. Hao, W. Yang, Y. Xu, et al., Biosens. Bioelectron. 212 (2022) 114411.
[5] M. Hu, X. Hu, G. Wang, et al., Food Chem. 419 (2023) 136025.
[6] Y. Huang, S. Zhang, Q. Zheng, et al., Clin. Chim. Acta 488 (2019) 202–208.
[7] R. Hu, T. Liao, Y. Ren, et al., Nano Res. 15 (2022) 7313–7319.
[8] L.J. Ao, T. Liao, L. Huang, et al., Chem. Eng. J. 436 (2022) 135204.
[9] R. Chen, X.B. Zhou, Y. Wu, et al., Sens. Actuators B: Chem. 328 (2021) 129050.
[10] S. He, J. Song, J. Qu, et al., Chem. Soc. Rev. 47 (2018) 4258–4278.
[11] M. Zhao, B. Li, H. Zhang, et al., Chem. Sci. 12 (2020) 3448–3459.
[12] H.H. Han, H. Tian, Y. Zang, et al., Chem. Soc. Rev. 50 (2021) 9391–9429.
[13] Y.Q. Chen, J. Chen, B.S. Chang, Iradiology 1 (2023) 36–40.
[14] Z. Yu, C. Eich, L.J. Cruz, Front. Chem. 8 (2020) 496.
[15] L. Li, Z. Zeng, Z. Chen, et al., ACS Nano 14 (2020) 15403–15416.
[16] Z. Song, Y. Suo, S. Duan, et al., Biosens. Bioelectron. 224 (2023) 115063.
[17] Y. Fan, F. Zhang, Adv. Opt. Mater. 7 (2019) 1801417.
[18] S. He, S. Chen, D. Li, et al., Nano Lett. 19 (2019) 2985–2992.
[19] Y. Sun, W. Zhang, B. Wang, et al., Chem. Commun. 54 (2018) 3851–3854.
[20] S. Lahtinen, A. Lyytikäinen, H. Päkkilä, et al., J. Phys. Chem. C 121 (2017) 656–665.
[21] C. Cao, M. Xue, X. Zhu, et al., ACS Appl. Mater. Interfaces 9 (2017) 18540–18548.
[22] Z. Song, H. Guo, Y. Suo, et al., ACS Appl. Mater. Interfaces 15 (2023) 52038–52050.
[23] A.T. Kal-Koshvandi, TRAC Trend. Anal. Chem. 128 (2020) 115920.
[24] X.J. Xie, N.Y. Gao, R.R. Deng, et al., J. Am. Chem. Soc. 135 (2013) 12608–12611.
[25] R. Wang, X.M. Li, L. Zhou, et al., Angew. Chem. Int. Ed. 53 (2014) 12086–12090.
[26] G.Y. Chen, J. Damasco, H.L. Qiu, et al., Nano Lett. 15 (2015) 7400–7407.
[27] D. Li, S. He, Y. Wu, et al., Adv. Sci. 6 (2019) 1902042.
[28] Y.F. Wang, G.Y. Liu, L.D. Sun, et al., ACS Nano 7 (2013) 7200–7206.
[29] B.T. Bajar, E.S. Wang, S. Zhang, et al., Sensors 16 (2016) 1488.
[30] X.M. Zou, Y. Liu, X.J. Zhu, et al., Nanoscale 7 (2015) 4105–4113.
[31] Q. Song, L. Zhao, W. Mai, et al., Biosens. Bioelectron. 234 (2023) 115353.
[32] F. Liu, H. Chen, D. Deng, et al., Bioelectrochemistry 147 (2022) 108200.